

*DEFINE_PRESSURE_TUBE: simulating pressure tube sensors in pedestrian crash

Jesper Karlsson¹
¹DYNAmore Nordic AB

1 Introduction

This paper presents the new keyword ***DEFINE_PRESSURE_TUBE**, designed to efficiently simulate pressure waves in a thin air-filled tube. The main application in mind is a crash detection system for pedestrian safety, where an air-filled tube is embedded in the front bumper and fitted with pressure sensors at the ends, see Figure 1. In the case of an impact, the tube is compressed and a pressure wave travels to the sensors, enabling localization and extent of the impact. In recent years, such systems have gained popularity in the automotive industry, posing a challenging task in efficient and accurate simulations. The aim of this paper is to give an overview of the theory and usage of the keyword, as well as to show comparisons with experiments and existing methods in LS-DYNA.

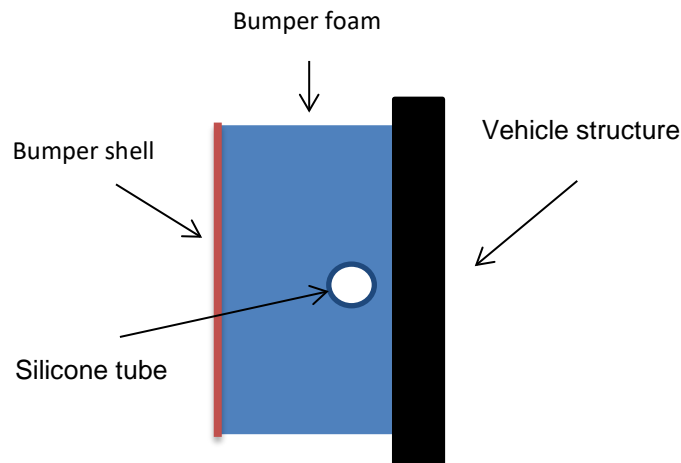


Fig. 1: Schematics of bumper cross section with embedded tube.

2 Keyword input and database output

The ***DEFINE_PRESSURE_TUBE** keyword defines a closed gas filled tube using tubular beam elements and the pressure is calculated from area changes, in time and space, given by contact penetration from surrounding elements. Currently only mortar contacts are supported.

Input data are given as below:

Card 1	1	2	3	4	5	6	7	8
Variable	PID	WS	PR	MTD	ATYPE			
Type	I	F	F	I	I			
Default	0	0.0	0.0	0	0			

Optional card:

Card 2	1	2	3	4	5	6	7	8
Variable	VISC	CFL	DAMP					
Type	F	F	F					
Default	1.0	0.9	0.0					

Only the first three parameters on card one are compulsory:

- **PID:** Part ID of tube. The tube(s) consists of all the beam elements in the part. Only ELFORM = 1,4,5,11 are allowed. Each set of joint beam elements in the part will model a tube and the beam elements may not contain junctions. Also, two different parts where *DEFINE_PRESSURE_TUBE is applied may not share beam nodes. For MPP all elements in the part will be on a single processor, therefore it is recommended that the part should only contain beam elements.
- **WS:** Wave propagation speed.
- **PR:** Initial tube pressure.

Parameter 4 and 5 concerns solver type and tube area calculation:

- **MTD:** Solution method. Only one method is currently supported (MTD=0), described in Sections 3 and 4.
- **ATYPE:** Type of cross section area calculation of the tube. Initial area is given by the diameter on *SECTION_BEAM. If both inner and outer diameter is given, the inner diameter is used, otherwise the outer diameter.
 0. Mortar contact penetration distance gives the minor axis of an ellipse with constant circumference, calculated from the initial area.
 1. Mortar contact penetration distance gives the radius of a perfectly circular tube.

For MTD=0 and extra optional card may be given:

- **VISC:** Artificial viscosity factor. Multiplies ϵ in Section 5.
- **CFL:** Time step factor for tube sub-stepping. Multiplies CFL in Section 5.
- **DAMP:** Linear damping factor to emulate pressure losses. Factor d in Section 5.

From a given PID, the solver will get the initial tube dimensions from the length and thickness of each beam element on that part. After initialization, the tube solver only uses penetration distance from the mortar contacts to calculate area over time, and is independent of the beam element deformation, i.e. it is assumed that the length of the tube is not too distorted over time. The tube solver uses a separate time integration routine, with time step size less than or equal to the global time step.

Pressure, density, velocity and tube area are output through the keyword *DATABASE_PRTUBE, and can be visualized in LS-PREPOST.

3 The tube model

Pressure propagation is governed by a 1D model based on the compressible Euler equations, resulting in a very efficient method compared to 3D CFD or particle methods. This 1D model is derived in the following sections, based on [1].

3.1 Euler equations

The 1D Euler equations for a compressible inviscid fluid (in thermal equilibrium) are given in differential form by

$$\begin{aligned}\frac{\partial \rho}{\partial t} + \frac{\partial}{\partial x}(\rho u) &= 0, \\ \frac{\partial}{\partial t}(\rho u) + \frac{\partial}{\partial x}(\rho u^2 + p) &= 0, \\ \frac{\partial E}{\partial t} + \frac{\partial}{\partial x}(u(E + p)) &= 0,\end{aligned}$$

where the independent variables are: fluid density ρ , velocity u , energy per unit volume E , and pressure p . The energy E is related to the *internal energy per unit mass*, e , by

$$E = \rho e + \frac{\rho}{2} u^2.$$

That is, the energy per unit volume is composed of molecular internal energy (rotational, vibrational, translational, etc.) plus kinetic energy of the fluid flow.

Since we have three equations but four independent variables we need an extra equation to complete this system of equations. This can be done by an *equation of state*, in our case the *ideal gas law* for a *polytropic gas*

$$E = \frac{p}{(\gamma - 1)} + \frac{\rho}{2} u^2,$$

where $\gamma = c_p/c_v$ is the *adiabatic index*, c_p is the specific heat at constant pressure, and c_v is the specific heat at constant volume. The adiabatic index is approximately 1.4 for air.

Although stated in differential form, the above system is a system of conservation laws, describing the conservation of mass, momentum, and energy. Such systems allow complex (sometimes non-physical) phenomena to develop over time, e.g. shocks and rarefaction waves, particularly in the supersonic range when the fluid velocity u is close to the speed of sound

$$c := \sqrt{\left(\frac{\partial p}{\partial \rho}\right)_s} = \sqrt{\frac{K_s}{\rho}},$$

where K_s is the isentropic bulk modulus. In our application, we assume that we have smooth flows in the subsonic regime.

3.2 Isentropic Euler equations

Entropy is a measure of the disorder in the system and can be defined as

$$s := c_v \log \frac{p}{\rho^\gamma}.$$

One of the fundamentals of thermodynamics is that the entropy in a system must increase over time, a condition that is useful to weed out physical solutions to the Euler equations. Typically, the entropy increases when a particle passes through a shock wave.

From the entropy we deduce that

$$p(\rho, s) = \rho^\gamma e^{s/c_v},$$

and

$$\frac{\partial p}{\partial \rho} = \gamma \rho^{\gamma-1} e^{s/c_v} = \frac{\gamma p}{\rho}.$$

Also, from the definition of entropy, the energy equation in the Euler equations can be replaced by

$$\frac{\partial s}{\partial t} + u \frac{\partial s}{\partial x} = 0.$$

For smooth flows (e.g. acoustic waves) the entropy is constant along a particle path, i.e. the above equation is automatically satisfied. The Euler equations can then be reduced to the *isentropic Euler equations*

$$\begin{aligned} \frac{\partial \rho}{\partial t} + \frac{\partial}{\partial x}(\rho u) &= 0, \\ \frac{\partial}{\partial t}(\rho u) + \frac{\partial}{\partial x}(\rho u^2 + c^2 \rho / \gamma) &= 0, \end{aligned}$$

with sound speed

$$c := \sqrt{\frac{\gamma p}{\rho}}.$$

These equations still allow shocks to form, but such shocks lack physical meaning since the entropy is assumed constant along the flow.

3.3 Isothermal Euler equations

Assume constant entropy and let $c_v, c_p \rightarrow \infty$ such that $\gamma = c_p/c_v \rightarrow 1$. This corresponds to molecules with infinitely many degrees of freedom that can take up an infinite amount of energy without changing the temperature of the system. Thus, such a fluid will maintain a constant temperature.

From the isentropic Euler equations, we then get the *isothermal Euler equations*

$$\frac{\partial \rho}{\partial t} + \frac{\partial}{\partial x}(\rho u) = 0,$$

$$\frac{\partial}{\partial t}(\rho u) + \frac{\partial}{\partial x}(\rho u^2 + c^2 \rho) = 0,$$

and the pressure is proportional to the density through

$$p = c^2 \rho,$$

where the sound speed, c , is constant.

Although this is still a non-linear system, no shocks will develop over time for isentropic and isothermal flow.

3.4 Acoustic wave equation

For acoustic phenomena, it is assumed that variations in pressure, density, and velocity, are small perturbations $(\delta\rho, \delta p, \delta u)$, from a steady state (ρ_0, p_0, u_0) .

Let $u_0 = 0$, and $\rho = \rho_0 + \delta\rho$, then the isothermal Euler equations become

$$\begin{aligned} \frac{\partial \rho}{\partial t} + \frac{\partial}{\partial x}((\rho_0 + \delta\rho)u) &= 0, \\ \frac{\partial}{\partial t}((\rho_0 + \delta\rho)u) + \frac{\partial}{\partial x}((\rho_0 + \delta\rho)u^2 + c^2 \rho) &= 0, \end{aligned}$$

and if we ignore higher order terms we get the linearized equations

$$\begin{aligned} \frac{\partial \rho}{\partial t} + \rho_0 \frac{\partial u}{\partial x} &= 0, \\ \rho_0 \frac{\partial u}{\partial t} + c^2 \frac{\partial \rho}{\partial x} &= 0. \end{aligned}$$

Taking the temporal derivative of the first equation and the spatial derivative of the second gives, together with $\rho = p/c^2$, the classical wave equation

$$\frac{1}{c^2} \frac{\partial^2 p}{\partial t^2} - \frac{\partial^2 p}{\partial x^2} = 0.$$

3.5 Quasi-1D Euler equations

To utilize the above theory in the context of a pressure tube we need to consider the variation of the cross-section area of the tube. Thus, for a pipe of cross section area $A = A(x, t)$, we assume the volume change

$$dV(t) = A(x, t)dx + O(dx^2).$$

The conservation of mass along a segment $[x, x + dx]$ then becomes

$$\frac{\partial}{\partial t}(A\rho)dx + [A\rho u]_{x}^{x+dx} = 0,$$

which can be approximated by

$$\frac{\partial}{\partial t}(A\rho)dx + \frac{\partial}{\partial x}(A\rho u)dx = 0,$$

or in differential form

$$\frac{\partial}{\partial t}(A\rho) + \frac{\partial}{\partial x}(A\rho u) = 0.$$

Similarly, for the momentum equation, we have

$$\frac{\partial}{\partial t}(A\rho u) + \frac{\partial}{\partial x}(A\rho u^2) + A \frac{\partial p}{\partial x} = 0,$$

or

$$\frac{\partial}{\partial t}(A\rho u) + \frac{\partial}{\partial x}(A\rho u^2 + Ap) = p \frac{\partial A}{\partial x},$$

and for the energy equation we simply get

$$\frac{\partial}{\partial t}(AE) + \frac{\partial}{\partial x}(Au(E + p)) = 0.$$

To summarize, the full quasi-1D Euler equations for varying thickness are

$$\begin{aligned}\frac{\partial}{\partial t}(A\rho) + \frac{\partial}{\partial x}(A\rho u) &= 0, \\ \frac{\partial}{\partial t}(A\rho u) + \frac{\partial}{\partial x}(A\rho u^2 + Ap) &= p \frac{\partial A}{\partial x}, \\ \frac{\partial}{\partial t}(AE) + \frac{\partial}{\partial x}(Au(E + p)) &= 0,\end{aligned}$$

which correspond to the original Euler equations, but with a source term coming from the varying cross section area. These equations are described in [2].

3.6 Quasi-1D acoustic equations

The quasi-1D isothermal Euler equations become,

$$\begin{aligned}\frac{\partial}{\partial t}(A\rho) + \frac{\partial}{\partial x}(A\rho u) &= 0, \\ \frac{\partial}{\partial t}(A\rho u) + \frac{\partial}{\partial x}(A\rho u^2 + Ac^2\rho) &= p \frac{\partial A}{\partial x},\end{aligned}$$

and linearization around $(\rho_0, p_0, u_0 = 0)$ gives the acoustic approximation

$$\begin{aligned}\frac{\partial}{\partial t}(A\rho) + \rho_0 \frac{\partial y}{\partial x} &= 0, \\ \rho_0 \frac{\partial y}{\partial t} + c^2 \frac{\partial}{\partial x}(A\rho) &= p \frac{\partial A}{\partial x},\end{aligned}$$

where $y = Au$. Expressed in y and p we have

$$\begin{aligned}\frac{\partial p}{\partial t} + \frac{\partial \ln A}{\partial t} p + \frac{p_0}{A} \frac{\partial y}{\partial x} &= 0, \\ \frac{\partial y}{\partial t} + A \frac{c^2}{p_0} \frac{\partial p}{\partial x} &= 0.\end{aligned}$$

4 Numerics

To solve the acoustic approximation of the quasi-1D Euler equations we use the simplest possible method for advection problems on variable meshes, i.e. the continuous Galerkin method with artificial viscosity.

In semi-discrete form, the continuous Galerkin method is

$$\begin{bmatrix} \mathbf{M} & \mathbf{0} \\ \mathbf{0} & \mathbf{M} \end{bmatrix} \frac{d}{dt} \begin{bmatrix} \mathbf{p} \\ \mathbf{y} \end{bmatrix} + \begin{bmatrix} \mathbf{M}_A(t) & p_0 \mathbf{K}_A(t) \\ \frac{c^2}{p_0} \mathbf{K}_B(t) & \mathbf{0} \end{bmatrix} \begin{bmatrix} \mathbf{p} \\ \mathbf{y} \end{bmatrix} = \begin{bmatrix} \mathbf{0} \\ \mathbf{0} \end{bmatrix},$$

with nodal solution variables

$$\begin{aligned}\mathbf{p} &= (p_0, p_1, \dots, p_{N-1}, p_N), \\ \mathbf{y} &= (A_0 u_0 = 0, A_1 u_1, \dots, A_{N-1} u_{N-1}, A_N u_N = 0).\end{aligned}$$

The mass and stiffness matrices are given by

$$\begin{aligned}\mathbf{M}_{ij} &= \int \phi_i \phi_j dx, \\ (\mathbf{M}_A)_{ij} &= \int \frac{\partial \ln A}{\partial t} \phi_i \phi_j dx, \\ (\mathbf{K}_A)_{ij} &= \int \frac{\phi'_i \phi_j}{A} dx, \\ (\mathbf{K}_B)_{ij} &= \int A \phi'_i \phi_j dx,\end{aligned}$$

with nodal basis functions ϕ_i .

This system is strictly hyperbolic with the distinct real eigenvalues

$$\lambda_{1,2}(t) = \frac{\Delta x}{2} \frac{\partial \ln A}{\partial t} \pm \sqrt{\left(\frac{\Delta x}{2} \frac{\partial \ln A}{\partial t}\right)^2 + c^2},$$

and gives the CFL condition

$$\Delta t(t) < \frac{\Delta x}{\max(\lambda_1(t), \lambda_2(t))} \leq \frac{\Delta x}{\Delta x \left| \frac{\partial \ln A}{\partial t} \right| + c}.$$

This condition is only necessary, not necessarily sufficient, for the convergence of an explicit one-step method. It makes sure that the time it takes for a wave of speed $\lambda_{1,2}$ to pass a computational domain of size Δx is longer than the computational time step Δt . Thus, the computational solution has a reasonable chance to keep up with the wave.

Adding artificial diffusion of size ϵ leads to the system

$$\begin{bmatrix} \mathbf{M} & \mathbf{0} \\ \mathbf{0} & \mathbf{M} \end{bmatrix} \frac{d}{dt} \begin{bmatrix} \mathbf{p} \\ \mathbf{y} \end{bmatrix} + \begin{bmatrix} \mathbf{M}_A(t) + \epsilon \mathbf{S} & p_0 \mathbf{K}_A(t) \\ \frac{c_0^2}{p_0} \mathbf{K}_B(t) & \epsilon \mathbf{S} \end{bmatrix} \begin{bmatrix} \mathbf{p} \\ \mathbf{y} \end{bmatrix} = \begin{bmatrix} \mathbf{0} \\ \mathbf{0} \end{bmatrix},$$

where

$$S_{ij} = \int \phi'_i \phi'_j dx.$$

The CFL condition now becomes

$$\Delta t(t) < \frac{\Delta x}{\max(\lambda_1(t), \lambda_2(t))} \leq \frac{\Delta x}{\frac{2\epsilon}{\Delta x} + \Delta x \left| \frac{\partial \ln A}{\partial t} \right| + c} =: CFL,$$

and to prevent unnecessarily small $\Delta t(t)$ for small Δx , we set

$$\epsilon = c\Delta x.$$

Optional linear damping of size d adds yet another term:

$$\begin{bmatrix} \mathbf{M} & \mathbf{0} \\ \mathbf{0} & \mathbf{M} \end{bmatrix} \frac{d}{dt} \begin{bmatrix} \mathbf{p} \\ \mathbf{y} \end{bmatrix} + \begin{bmatrix} \mathbf{M}_A(t) + \epsilon \mathbf{S} & p_0 \mathbf{K}_A(t) \\ \frac{c_0^2}{p_0} \mathbf{K}_B(t) & \epsilon \mathbf{S} \end{bmatrix} \begin{bmatrix} \mathbf{p} \\ \mathbf{y} \end{bmatrix} + \begin{bmatrix} d\mathbf{M}(\mathbf{p} - p_0) \\ \mathbf{0} \end{bmatrix} = \begin{bmatrix} \mathbf{0} \\ \mathbf{0} \end{bmatrix},$$

Time integration is done with Heun's method, a second order Runge-Kutta method,

$$\begin{aligned} \begin{bmatrix} \tilde{\mathbf{p}} \\ \tilde{\mathbf{y}} \end{bmatrix}_{n+1} &= \begin{bmatrix} \mathbf{p} \\ \mathbf{y} \end{bmatrix}_n - \Delta t \begin{bmatrix} \mathbf{M}_A(t_n) + \epsilon \mathbf{S} & p_0 \mathbf{K}_A(t_n) \\ \frac{c_0^2}{p_0} \mathbf{K}_B(t_n) & \epsilon \mathbf{S} \end{bmatrix} \begin{bmatrix} \mathbf{p} \\ \mathbf{y} \end{bmatrix}_n, \\ \begin{bmatrix} \mathbf{p} \\ \mathbf{y} \end{bmatrix}_{n+1} &= \begin{bmatrix} \mathbf{p} \\ \mathbf{y} \end{bmatrix}_n - \frac{\Delta t}{2} \left(\begin{bmatrix} \mathbf{M}_A(t_n) + \epsilon \mathbf{S} & p_0 \mathbf{K}_A(t_n) \\ \frac{c_0^2}{p_0} \mathbf{K}_B(t_n) & \epsilon \mathbf{S} \end{bmatrix} \begin{bmatrix} \mathbf{p} \\ \mathbf{y} \end{bmatrix}_n + \begin{bmatrix} \mathbf{M}_A(t_{n+1}) + \epsilon \mathbf{S} & p_0 \mathbf{K}_A(t_{n+1}) \\ \frac{c_0^2}{p_0} \mathbf{K}_B(t_{n+1}) & \epsilon \mathbf{S} \end{bmatrix} \begin{bmatrix} \tilde{\mathbf{p}} \\ \tilde{\mathbf{y}} \end{bmatrix}_{n+1} \right). \end{aligned}$$

5 Validation

As test example, a mass is dropped onto a 1.7 m long silicone tube with inner diameter 4 mm and outer diameter 8 mm, see Figure 2. The impactor and the support are approximated as rigid bodies, and the impactor is constrained to only allow translational movement in the x-direction, while the support is completely fixed. The tube is fixed at the two ends, as well as halfway between the point of impact and the ends. Experimental data were provided by Volvo Car Corporation.

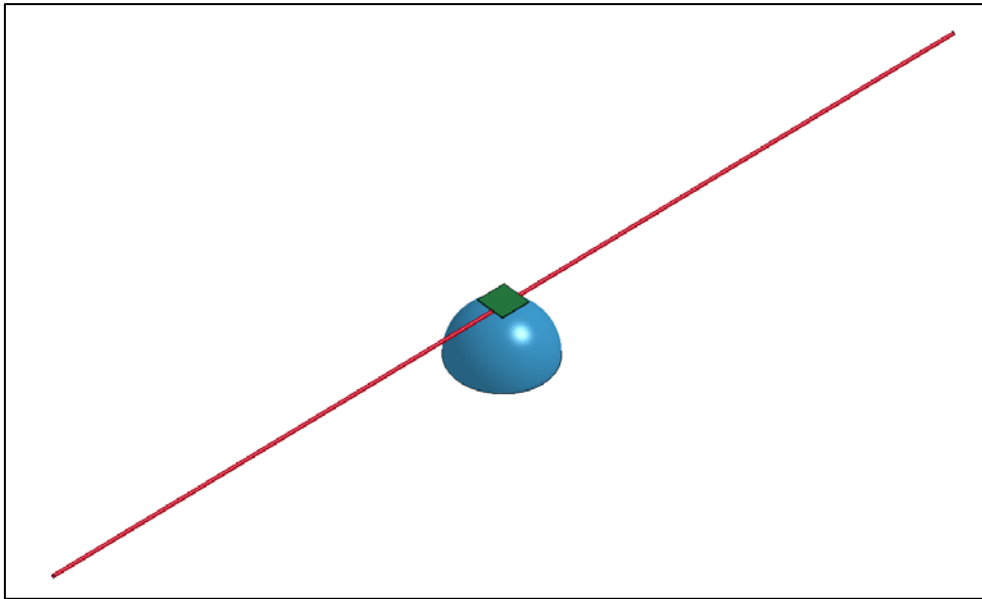


Fig.2: Tube test geometry for the embedded pressure tube. A mass is dropped from above with an initial downwards velocity of 10 km/h. The support (blue) is fixed. Rotational and sideways movement of the impactor (green) is restricted. The tube is fixed at the ends and around halfway between the ends and the point of impact.

Three approaches are tested (see Figure 3-6); the corpuscular particle method (CPM), the pressure tube embedded in a shell tube, and the pressure tube by itself:

1. **CPM:** This may be the most physically accurate method of the three since it models the interaction between “gas particles” and the structure, without any special assumptions on the tube geometry and tube-gas interaction. However, CPM generally gives noisy results and is quite expensive. In our examples the tube is modeled by shell elements and is filled with two million particles.
2. **Pressure tube only:** Here the tube is modeled using only beam elements. The tubular beam elements have both an inner and outer diameter, and models both structural tube response and pressure. Beam contact stiffness governs tube radial response and should be fitted to data w.r.t. penetration depth and velocity. Since contact stiffness gives a purely elastic response this may not be suitable for plastic deformation.
3. **Shell tube with embedded pressure tube:** Here tubular beam elements with inner diameter 0 are used, embedded inside a shell tube. The beam elements model air only, thus density and stiffness of the associated material are set to reasonably low values. Structural response is governed by the shell elements and the beam-to-shell contact stiffness corresponds to tube air pressure response.

Approximate run times for the different cases were:

1. **CPM:** 170 hours total CPU time.
2. **Pressure tube only:** 10 minutes total CPU time.
3. **Shell tube with embedded pressure tube:** 4 hours total CPU time.

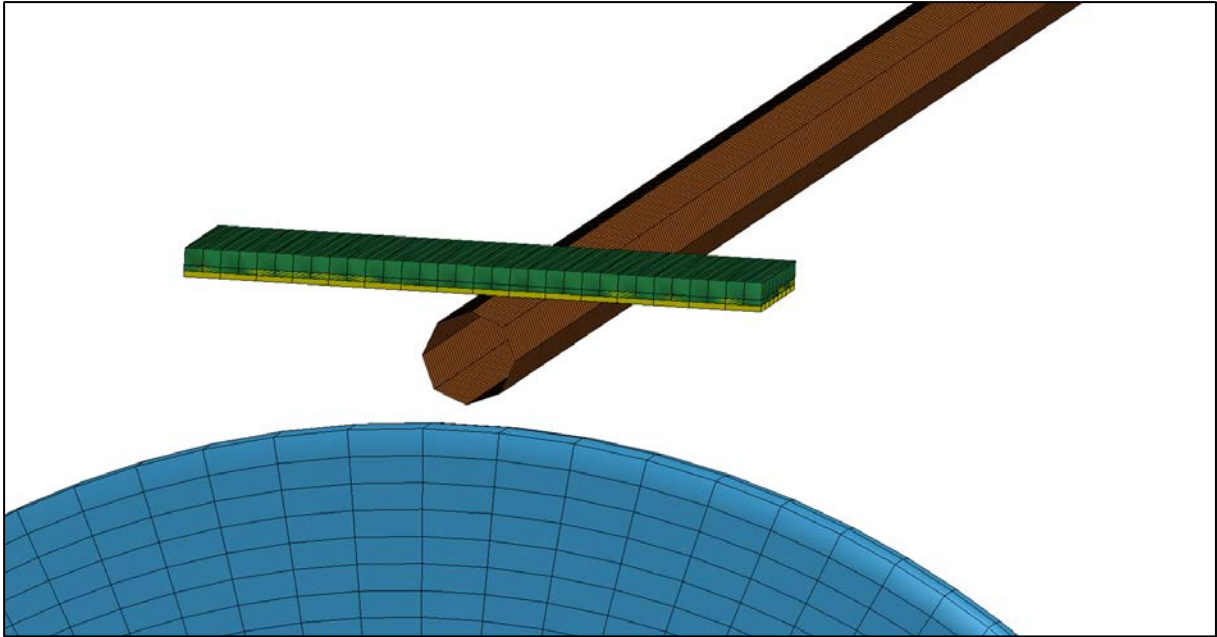


Fig.3: Initial cross sections for the hollow pressure tube. The pressure tube is here visualized using beam prisms and thickness of the shell elements is shown.

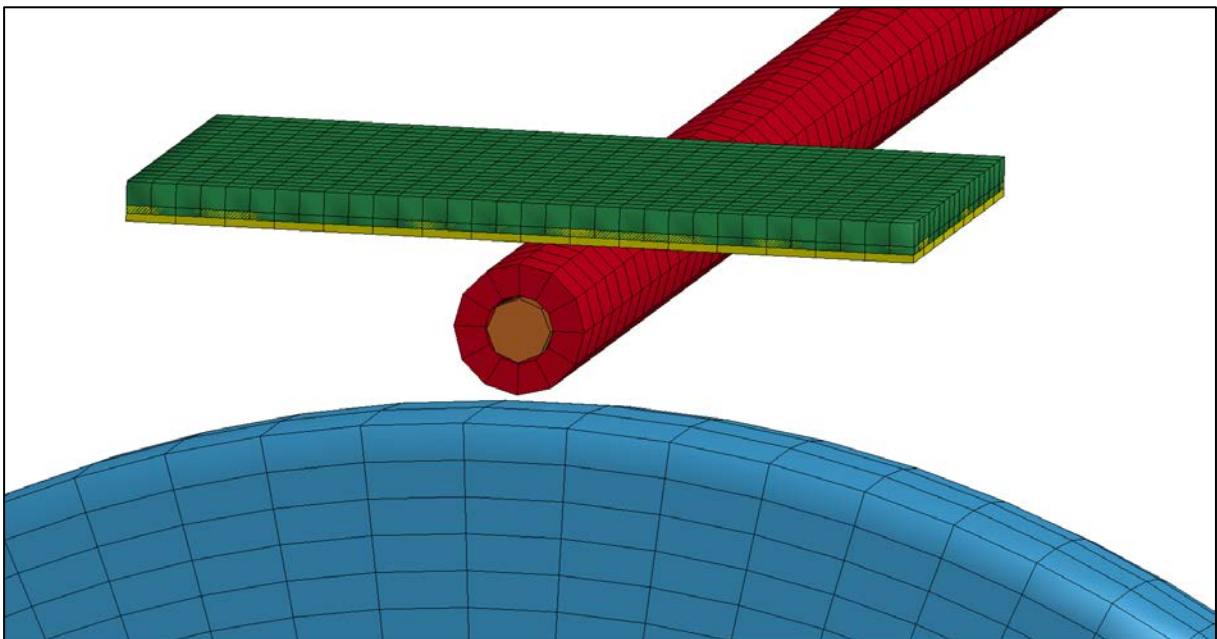


Fig.4: Initial cross section for the pressure tube embedded in a shell tube. The pressure tube is here visualized using beam prisms and thickness of the shell elements is shown.

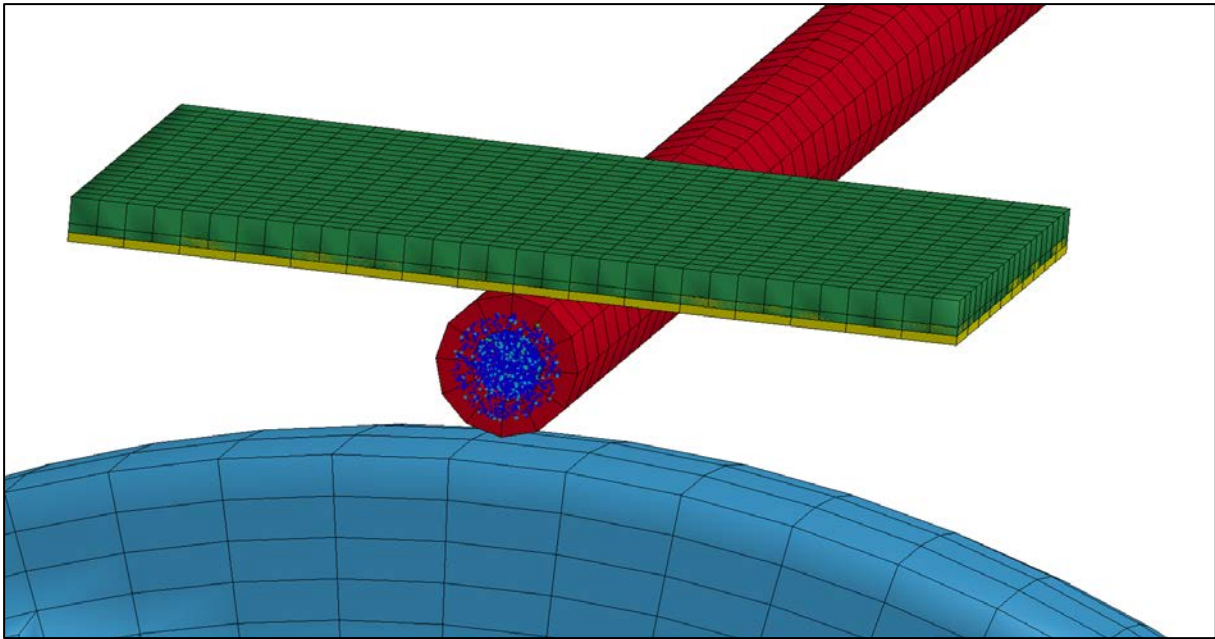


Fig.5: Cross section of the CPM shell tube filled with two million particles. Note that by the particles fill the tube all the way to the mid surface of the shell elements (here extruded), resulting in a larger volume. However, this still gives reasonable results. Another approach, better capturing the right cross section area, is found in Section 5.3.

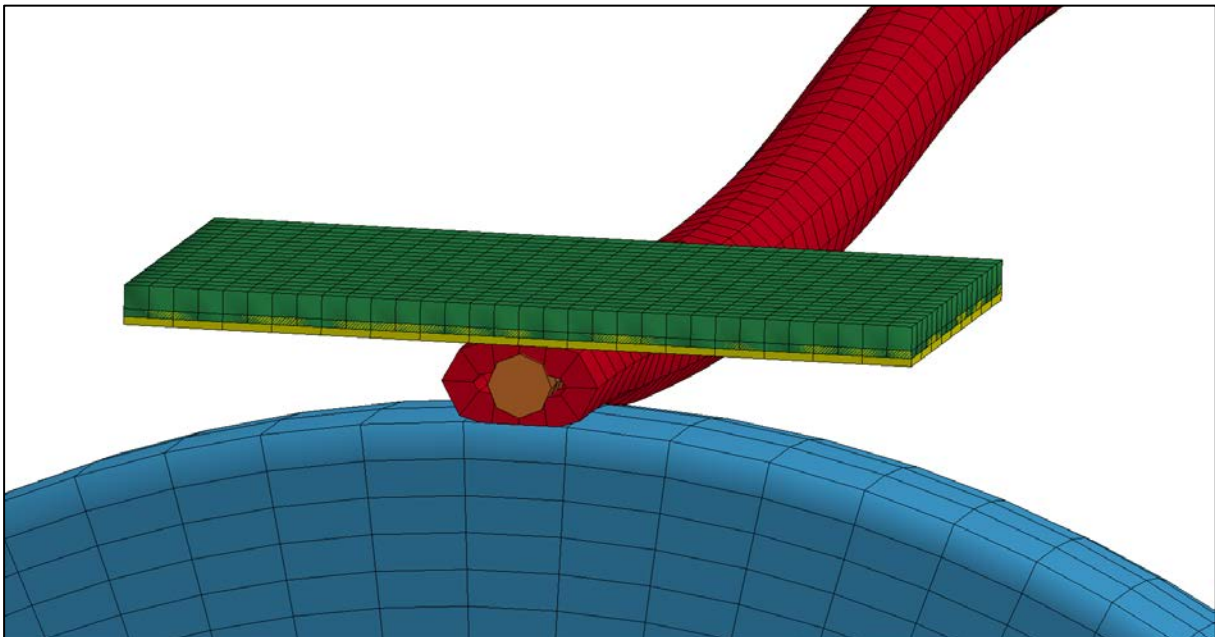


Fig.6: Cross section of the embedded pressure tube right after impact at 3ms. Here the penetration between the shells and the beams can be seen clearly.

5.1 Elastic tube

In this example, the impactor has an initial velocity of 10 km/h and the tube is modeled with **MAT_ELASTIC**. Impact will give rise to a pressure wave that bounces back and forth through the tube, and the pressure of interest is measured at the ends of the tube, see Figure 8. The wave speed here is much larger than the speed of deformation, and when the pressure wave comes back from being reflected at the ends, the impactor has bounced back and the tube has regained its shape. Tube

deformation in the impact location is visualized in Figure 7. Since the tube is fully elastic, the radial deformation can be approximated quite well with beam elements only.

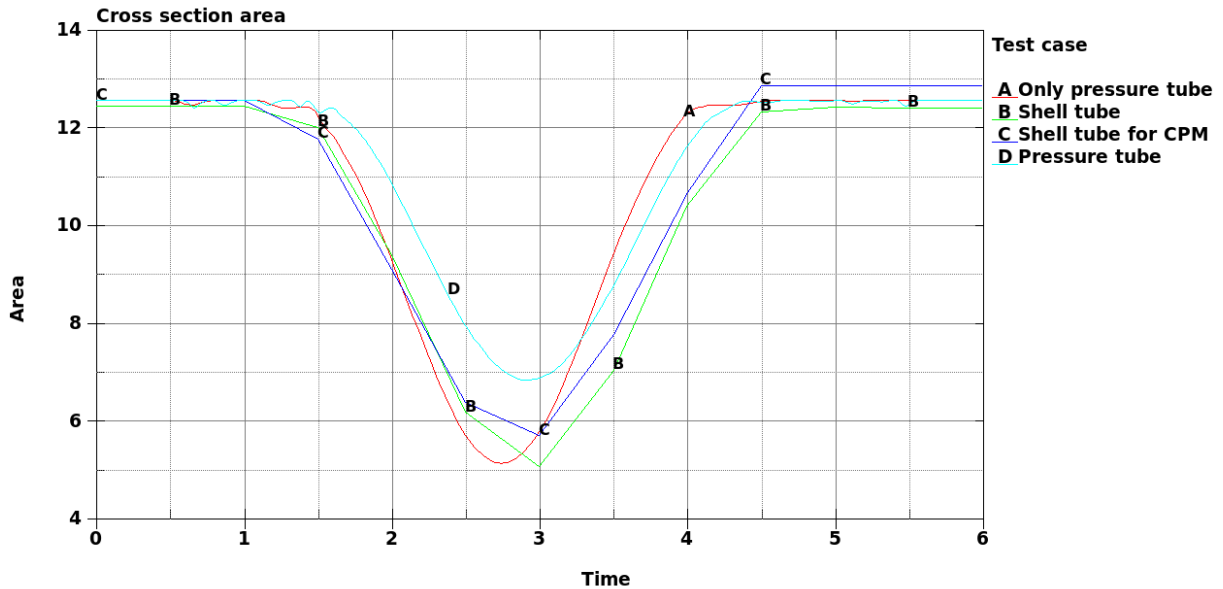


Fig.7: Cross section areas at location of impact (A: no shell tube, B+D: shell tube with embedded pressure tube, C: shell tube with CPM). Pressure tube area is calculated from contact penetration while shell tube area is estimated from geometry using the inner shell surface. It is evident that the pressure tube area when embedded in shell elements underestimates the area contraction, likely because a smaller beam radius gives inaccurate contact penetration. The contact stiffness parameters for the pressure tube without shells are here chosen by hand to give a similar area to the shell tube. Since the inner shell surface is used here, the actual area for CPM is greatly understated.

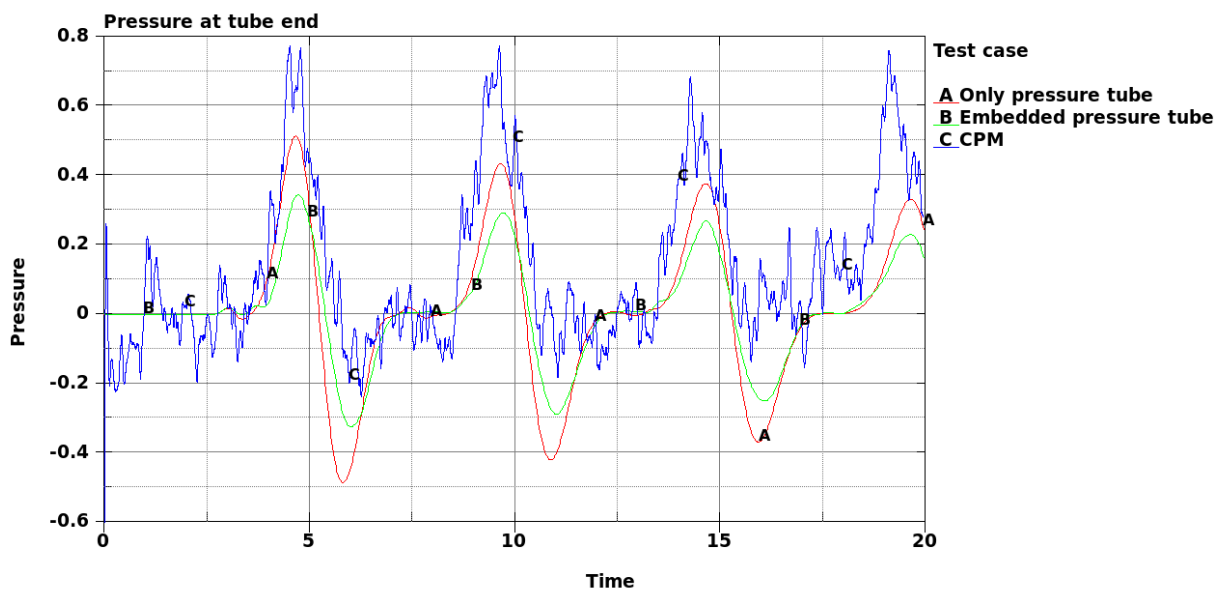


Fig.8: Pressure at end (normalized values). As expected from the area calculation, the embedded pressure tube underestimates the pressure. Using only the pressure tube without any shells also underestimates the pressure, but manages to capture the first pressure wave quite well, although the consequent reflections seem to be slightly out of phase.

5.2 Plastic tube

In this example, the impactor has an initial velocity of 10 km/h and the tube is modeled with `MAT_PIECEWISE_LINEAR_PLASTICITY`, using the same elasticity parameters as above. This plastic deformation agrees more with what is observed in experiments, although the tube may still be too stiff, as the experiments result in a completely compressed tube. Note that the radial plastic deformation of the tube cannot be modeled by the beam elements alone, see Figure 9.

The pressure wave for the tube enclosed in shells experiences less negative pressure than the pressure tube without shells, see Figure 10. However, the amplitude is again a bit lower. Note that all the simulations differ from the experimental data, which experiences no negative pressure at all. This is because the tested tube does not have any expansion at all after being fully compressed; essentially, it is being fused together.

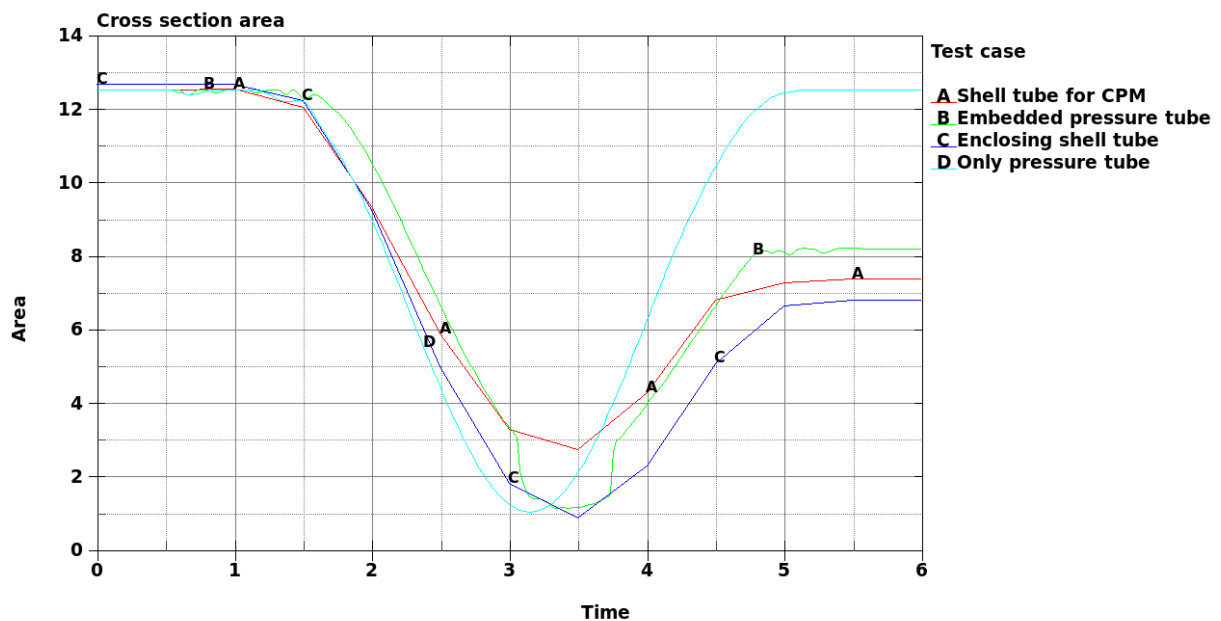


Fig.9: Cross section areas at location of impact for a plastic tube. It is here clear that the beam elements without surrounding shell structure cannot reproduce the correct radial response of the tube. Counterintuitively, the embedded pressure tube returns to a greater final area than the shell tube.

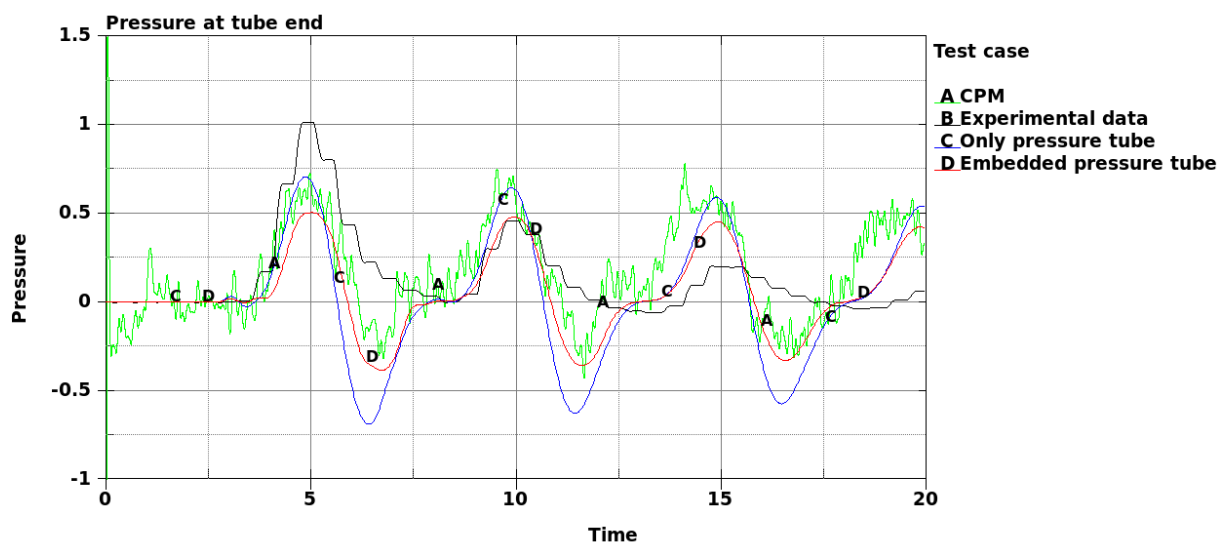


Fig.10: Pressure at end (normalized values), for plastic tube. All the simulation methods produce negative pressure, resulting from tube expansion, something that the test tube clearly lacks. The pressure wave in the test tube also have some damping that is not accounted for in the simulation models. Experimental data courtesy of Volvo Car Corporation.

5.3 CPM revisited

Since the particle volume in CPM is governed by the shell mid-surface, see Figure 5, the CPM simulations in previous sections gives too big cross section area. Thus, another approach is also tested, where an inner liner of weak thin shell elements is held in place with tied contacts, see Figure 11. This method gives significantly higher pressures, as in the experimental data, and gives more negative pressure from the expanding tube, see Figure 12 and 13. For some strange reason, CPM here gives a higher stationary pressure (1.1E5 Pa instead of 1.013E5 Pa), and for comparison the difference is subtracted.

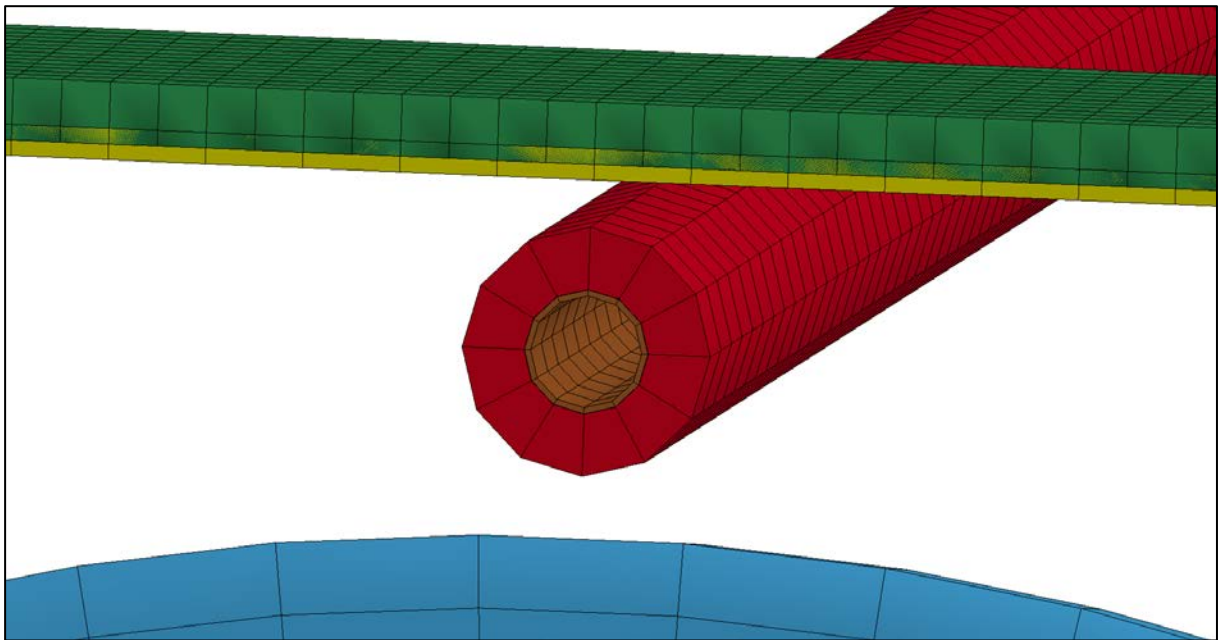


Fig.11: An inner liner of weak thin shell elements is created to limit the particle domain for CPM.

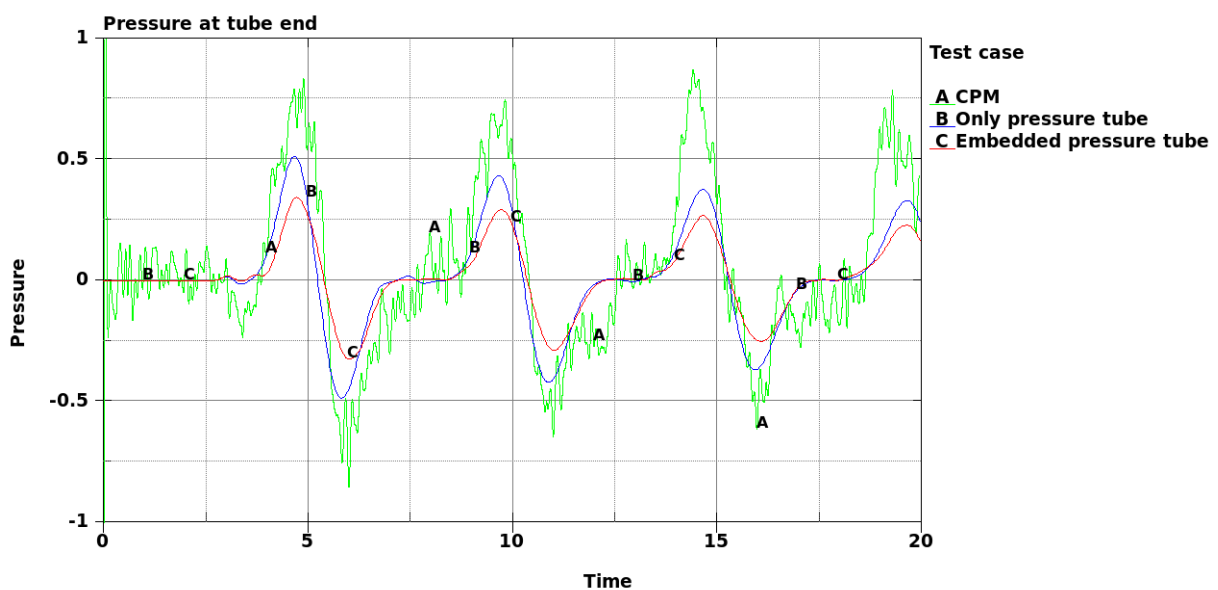


Fig.12: Comparison of pressures for elastic tube (normalized values). CPM now gives higher pressures and a more pronounced negative pressure for the tube expansion.

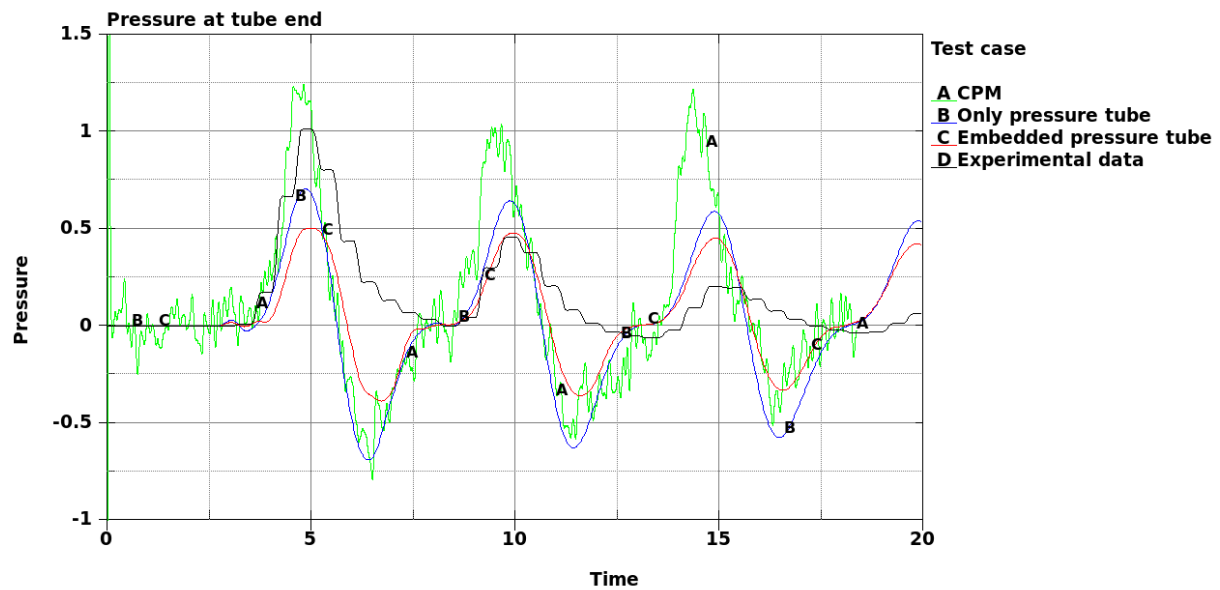


Fig.13: Comparison of pressures for plastic tube (normalized values).

6 Conclusions and future work

This paper presents the new keyword `*DEFINE_PRESSURE_TUBE`, designed to efficiently simulate pressure waves in a thin air-filled tube. The theory behind the keyword is based on a 1D acoustic approximation of the Euler equations, where the change in tube area acts as a source term for the pressure. Two different ways of modeling the tube are tested: beam elements with or without a surrounding shell structure. Validation against experimental data and simulations with the corpuscular particle method (CPM) shows that the 1D approximation fares well, at a fraction of the cost of CPM. However, both the 1D approximation and CPM need tuning to better capture experimental data. Future work includes validation with a tube embedded in foam, as well as improving the area estimation from the contact penetration.

7 Acknowledgements

Many thanks to Volvo Car Corporation for providing model parameters and experimental data.

8 References

- [1] R. J. LeVeque, *Finite-Volume Methods for Hyperbolic Problems*, Cambridge University Press, 2004.
- [2] T. H. Pulliam, "The Euler Equations," NASA Ames Research Center, 1994.